REYNOLDS NUMBER EFFECT ON THE HEAT TRANSFER MECHANISMS IN AIRCRAFT HOT AIR ANTI-ICE

Jean Fernando Bertão Machado, jeanbertao@hotmail.com
Cláudia Regina de Andrade, claudia@ita.br
Edson Luiz Zaparoli, zaparoli@ita.br
ITA - Instituto Tecnológico de Aeronáutica

Abstract. *The primary means of preventing ice formation on wings and engine inlets for modern commercial transport aircraft is by extracting hot air from the compressor and blowing it on the inside surface of the leading edge through small holes drilled in the so-called piccolo tube system. A critical aspect in the design of such system is the prediction of heat transfer of the impinging jets from the piccolo tube. The correct evaluation of the heat transfer rate in such devices is of great interest to optimize both the anti-icing performance and the hot air bleeding from the high-pressure compressor. A review of the literature reveals that there are some experimental and numerical studies that developed correlations for the average Nusselt number. However, most of the research was performed using a single jet or a group of jets impinging on a flat slat, which is different from the jet impingement on concave surfaces, as the inside surface of a wing. Therefore, the objective of the present work is use a commercial CFD software to perform a parametric study of the jet impingement on concave surfaces. The main goal is determine the effect of the Reynolds number on the heat transfer process. At the end of the work, a correlation for the average Nusselt number which account for the Reynolds number is presented.*

Keywords*: anti-icing hot air system, heat transfer, jet impingement, Reynolds number.*

1. INTRODUCTION

Atmospheric icing presents a major hazard to aircraft operating under natural icing conditions and is a cause of major concerns for the certification authorities and aircraft manufacturers. The steady rise in the global aviation traffic means an increased likelihood of encountering natural icing conditions. This suggests an increased frequency of icing related accidents unless a considerable amount of effort is focused on the various safety issues concerning in-flight aircraft icing.

In-flight icing is not only dangerous, but also has a major impact on the efficiency of flight operations. Rerouting and delays of commercial carriers, especially regional carriers and commuter airlines, to avoid icing conditions lead to late arrivals and the resulting ripple effect throughout the airspace traffic system. Diversions en route cause additional fuel and other costs for all classes of aircraft.

The icing formation has many effects on aircraft performance too. Ice or snow on the wing can reduce lift and increase drag. According to a work published by the Civil Aviation Authority (2000), research measurements taken on an aircraft with ice accretion disclosed a substantial increase of more than 60% in total drag and a loss of 17% in lift compared to a clean condition. These data were from a typical twin engine commuter type aircraft operation. If it is on leading edge, it may affect both of these to a greater degree. It may even change the point at which the airflow separates from the wing, altering the stall speed and stall characteristics of an airfoil.

All of these potential several problems point to the fact that, in many situations, significant icing is not permissible. Thus, to avoid these problems the aircrafts can be equipped with two types of ice protection systems: deicing systems and anti-icing systems. The deicing systems work periodically, waiting that a small portion of ice attach on a surface before remove. Mean while, the anti-icing systems are design to do not allow any formation of ice, working continually at any indication of icing.

The most prevalent deicing and anti-icing technique is the use of hot bleed air from the high-pressure compressor of the engine due to the availability of bleed and the reliability of the this technology. The hot air system is applied in the leading edges of the wing, tailplane and fin, empennages surfaces, radomes and jet engine air intakes. In general, the hot air is diverted from the source by interconnecting ductwork to the interior of the location to be anti iced or deiced. For wings or engine inlets, the air is discharged from the ductwork into piccolo tubes or narrow gap passages to transfer thermal energy to the aircraft skin along the chordwise direction. The spent air is then discharged overboard through ports in the aircraft skin. Fig. 1 shows an example of an anti-icing hot air system leading edge. The flow rate of hot air necessary for anti-icing or deicing is dependent on the source air temperature, heat losses through the ductwork, the geometry of the piccolo tube or narrow-gap passages and the parameters that effect ice accretion.

A correct evaluation of the heat transfer rate in the anti-icing hot air systems is of great interest to optimize both the anti-icing performance and the hot air bleeding from the high pressure compressor. Design parameters as the hole size and position or the specific mass flow could be carefully tuned from the knowledge of the temperature and flow fields.

However, the flow behavior within the slat is highly complex, as it spans both high speed supersonic jets as well as a very low Mach number core flow region. In addition, the heat transfer distribution along the inner side of the deicing surface is strongly influenced by the presence of large recirculating regions. Furthermore, three-dimensional effects can be significant.

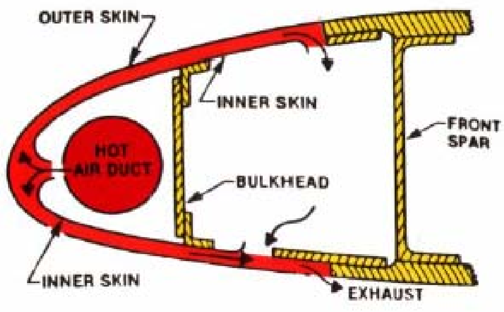

Figure 1 – Anti-icing hot air system leading edge

The majority of previous studies have focused on flat-surface impingement with various configurations of single or arrays of round and slot nozzles (Goldstein and Timmers, 1982; Huber and Viskanta, 1994; Lee and Lee, 1999; San and Lai, 2001; Ekkad et al, 2000; Tawfek, 2002). In general, works dealing with jets impinging on curved surfaces are limited, compared to flat-plate investigations, and the experiments performed by different investigators (Gau and Chung, 1991; Fregeau et al, 2005) have sometimes been contradictory, due to the differences in the experimental set-up conditions. Besides, there is not a unique correlation that takes account all the parameters that affect the heat transfer problem.

A Nusselt number correlation for the anti-icing thermal protection system was proposed by Zaparoli et al (2006). However, in this correlation the authors do not that account the effects of Reynolds number, which is a dimensionless parameter that often appear in the correlations.

Therefore, the main purpose of this work is to use the commercial CFD software FLUENT to perform a simulation of a jet impingement heat process on a cylindrical curved surface to investigate the influence of the jet Reynolds number in this problem.

2. MATHEMATICAL MODEL

2.1. Problem Description

In the thermal icing protection system, air from the turbine engine is channeled through a series of high temperature ducts and control valves system that supply the necessary hot air through the aircraft. A piccolo tube is the part of the thermal icing protection system that provides heated air to the leading section of an aircraft wing. In order to obtain the detailed insight required to analyze the heat transfer characteristics in this kind of anti-icing system, a series of CFD solutions were obtained for a simplified configuration: a single array of round jet impinging on a concave surface (see Figs 2 and 3). The jet emerges from a hole of diameter d with a jet spacing of c_n and a jet to wall distance of z_n. The piccolo tube diameter is D_p and the inner diameter of the concave surface is D_s.

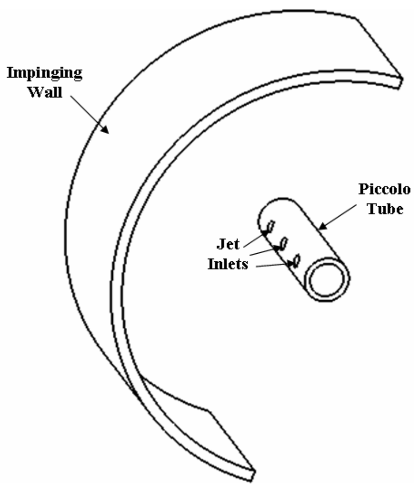

Figure 2 – Sketch of the impingement jet study.

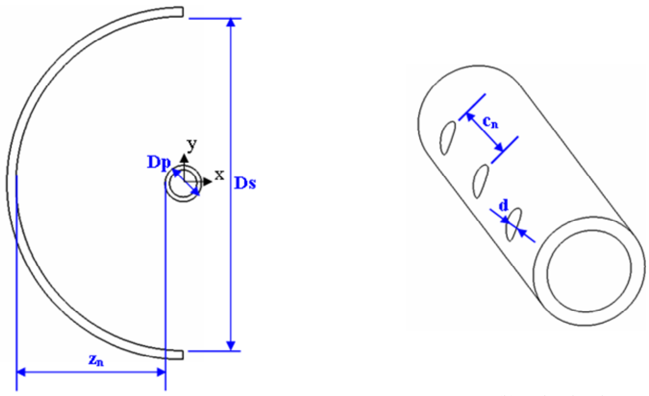

(a) – Front view

(b) – Piccolo tube detailed

Figure 3 – Geometric parameters for impingement jet present study

2.2. Governing equations

The present analysis is based on the conservation laws of mass, momentum and energy and the equation of state, considering that: i) steady state, ii) constant transport properties; iii) no internal heat generation; iv) effects of body forces and viscous dissipation are negligible. The following equations are obtained:

- Continuity

$$\frac{\partial}{\partial X_i}(\rho \vec{V}_i) = 0 \tag{1}$$

where ρ is the specific mass, $\vec{V}$ is the flow velocity, X is the coordinate and i = 1,2,3, which correspond, respectively, to the x-direction, y-direction and z-direction.

- Momentum or Navier-Stokes equations:

$$\frac{\partial}{\partial X_i}(\rho \vec{V}_i \vec{V}_j) = -\frac{\partial P}{\partial X_i} + \frac{\partial \tau_{ij}}{\partial X_j} \tag{2}$$

where j = 1,2,3, which correspond, respectively, to the x-direction, y-direction and z-direction, P is the pressure and τ_{ij} is the stress tensor.

- Energy equations:

$$\frac{\partial}{\partial X_i}(\rho \vec{V}_i h) = -\frac{\partial \vec{q}_i}{\partial X_i} \vec{V}_i \frac{\partial P}{\partial X_i} + \tau_{ij} \frac{\partial \vec{V}_j}{\partial X_i} \tag{3}$$

where h is the convective heat transfer coefficient and q_i is the heat flux vector, given by:

$$\vec{q}_i = -k \frac{\partial T}{\partial X_i} \tag{4}$$

where k is the thermal conductivity and T is the temperature.

- Energy of State:

$$P = \rho RT \tag{5}$$

where R is the ideal gas constant.

2.3. Turbulence Modeling

This problem was solved using the realizable $k-\varepsilon$ model with the Enhanced Wall Treatment to model the turbulence features.

The realizable $k-\varepsilon$ model was developed by Shih et al. (1995).The model transport equations for k and ε in the realizable $k-\varepsilon$ model are:

$$\frac{\partial(\rho V_i k)}{\partial x_i}=\frac{\partial}{\partial x_i}\left[\left(\mu+\frac{\mu_T}{\sigma_k}\right)\frac{\partial k}{\partial x_i}\right]-\rho\overline{V_iV_j}\frac{\partial V_i}{\partial x_j}-\rho\varepsilon \tag{6}$$

$$\frac{\partial(\rho V_i \varepsilon)}{\partial x_i}=\frac{\partial}{\partial x_i}\left[\left(\mu+\frac{\mu_T}{\sigma_\varepsilon}\right)\frac{\partial \varepsilon}{\partial x_i}\right]+\rho C_1 S\varepsilon-\rho C_2\frac{\varepsilon^2}{k+\sqrt{\nu\varepsilon}} \tag{7}$$

where k is the turbulent kinetic energy, ε is the dissipation rate, μ is the dynamic viscosity, μ_T is the eddy viscosity, ν is the cinematic viscosity, $C_1 = max\left[0.43,\frac{\eta}{\eta+5}\right]$, $\eta = S\frac{k}{\varepsilon}$; $S=\sqrt{2S_{ij}S_{ij}}$, $S_{ij}=\frac{1}{2}\left(\frac{\partial V_i}{\partial x_j}+\frac{\partial V_j}{\partial x_i}\right)$,.$C_2$ = 1.9, σ_k = 1.0 and σ_ε = 1.2.

2.4. Boundary Conditions

The imposed boundary conditions are shown in Fig. 4.

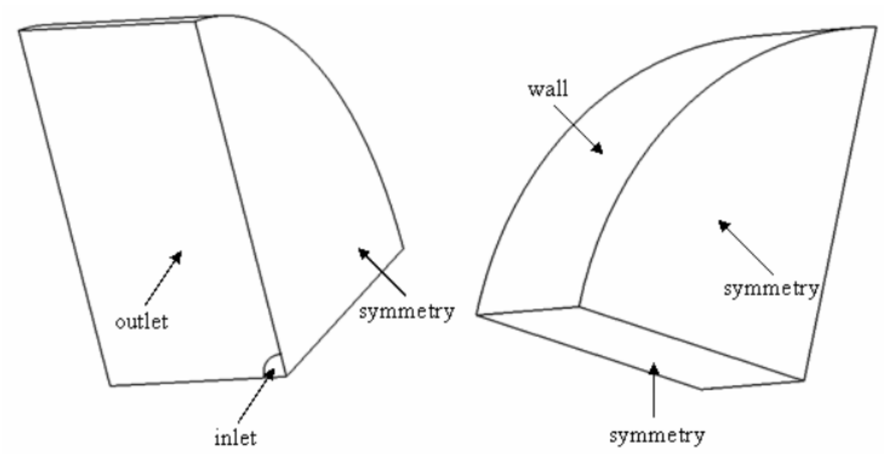

Figure 4 – Boundary conditions

For the CFD simulations, symmetry was specified in the spanwise direction and through the middle of the piccolo jet. On the impinging wall, a no-slip constant temperature condition was imposed. A pressure boundary condition was set at the inlet and outlet. In order to produce a fluid velocity of 0.4 Ma and to maintain a jet inlet static temperature of 300 K, a total temperature (T_T) and a total relative pressure (P_{TR}) was set at the hole inlet according to the following equations:

$$\frac{T_T}{T}=1+\frac{(\gamma-1)}{2}\cdot M^2 \tag{8}$$

$$\frac{P_T}{P}=\left[1+\frac{(\gamma-1)}{2}\cdot M^2\right]^{\frac{\gamma}{\gamma-1}} \tag{9}$$

$$P_{TR}=P_T-P \tag{10}$$

where T_T is the total temperature, T is the inlet static temperature, γ is the specific heat ratio, Ma is the Mach number, P_T is the total pressure, P is the inlet static pressure, and P_{TR} is the total relative pressure.

Considering an inlet static pressure of 101,325 Pa and a specific heat ratio of 1.4, the above equations will lead to a total temperature of 309.6 K and a total relative pressure of 11,809.6 Pa.

Also, the conditions were uniform across the hole inlet (i.e. no variable profiles were specified). The outlet is treated as a zero-pressure boundary and at a temperature of 280 K. The impinging surface is maintained with a constant temperature of 280 K. In addition, the turbulence intensity was set to 5% and the turbulence viscous ratio was set to 30%.

3. RESULTS

3.1. Model Validation

The validation of a numerical results is difficulty due to the fact that details of most of the experimental data sets are not known, or to the fact that the geometry and boundary conditions are not well posed. The work founded during the literature review that shows the most similarity with the present study was the work developed by Zaparoli et al. (2006). Therefore, to establish the validation of our CFD model, the Zaparoli et al. (2006) study has been used for comparison.

As mentioned in the literature review, the Zaparoli et al. (2006) work analyzes the anti-icing thermal protection system for wing leading edge and provides a Nusselt number correlation to evaluate the heat transfer rate for a preliminary design of this anti-icing system. This correlation is shown in the Equation below:

$$\overline{Nu} = 689.2152(Ma)^{0.69916}\left(\frac{c_n}{d}\right)^{-0.4264}\left(\frac{z_n}{d}\right)^{-0.9385} \tag{11}$$

where $\overline{Nu}$ is the average Nusselt number. As the correlation presented provides the average Nusselt number, this is the parameter used for the validation.

The average Nusselt number is defined as:

$$\overline{Nu} = \frac{1}{A}\int_A (Nu)dA \tag{12}$$

where A is impingement surface area and Nu is the local Nusselt number, which is calculated as:

$$Nu(x,y) = \frac{h(x,y)\cdot D_s}{k} \tag{13}$$

where Ds is the impingement surface diameter, k is the thermal conductivity and h is the local convection heat coefficient, given by:

$$h(x,y) = \frac{q_s(x,y)}{(T_{tota} - T_s)} \tag{14}$$

where qs is the impinging surface local heat flux.

The numerical simulation for the validation case was performed using a Mach number Ma = 0.4 and a jet inlet static temperature T_{in} = 300 K, which correspond to a total temperature T_T = 309.6 K and a total relative pressure of P_{TR} = 11,809.6 Pa at the inlet. The impinging surface is maintained with a constant temperature T_w = 280 K. A summary of the input conditions for the validation case is in Tab. 1.

Table 1 – Parameters used in the validation case

Ma	d (mm)	z_n/d	c_n/d	$\Delta T(T_{in} - T_w)$
0.4	6.35	6	16	20

Three meshes (coarse, intermediate and refined) were generated for the validation case. The number of cells and the average Nusselt number results for each mesh is shown in Tab. 2. The refined mesh is used to compare the average Nusselt number results.

Table 2 – Average Nusselt number mesh sensitivity

	Number of cells		
	Coarse	Intermediate	Refined
Number of cells	131,731	312,303	577,007
Average Nusselt Number	24.71	24.90	24.22
Difference	2.02 %	2.81 %	0

As we can see, the difference between the three meshes is low, which means that the grid is not affecting the result. The average Nusselt number obtained in the present work and the value resulted from the Zaparoli et al. (2006) correlation, Eq.(11), are shown in Tab. 3.

Table 3 – Comparison of average Nusselt number for impingement jet in a concave surface

	Zaparoli et al. (2006)	Present study
Average Nusselt Number	20.99	24.22
Difference	0	15.38%

The difference between the results accounts to 15.38%, which can be considered as a reasonable agreement once the correlation provided by Zaparoli et al. (2006) also carries an inherent discrepancy (it was obtained from a curve fitting over their numerical results).

3.2. Present work results

After a dimension analysis, the Nusselt number correlation should take account the effect of the parameters indicated in Equation 15:

$$Nu = \frac{hl}{k} = f\left(arrangement, \frac{x}{l}, \frac{y}{l}, \alpha, \beta, \theta, N_\beta, \frac{c_n}{l}, \frac{z_n}{l}, \frac{D_s}{l}, \frac{D_p}{l}, \frac{e}{l}, Re, Ma, \frac{P_{jet}}{P_{atm}}, Pr, Ec, bc, S \right) \tag{15}$$

where arrangement is the system configuration (holes relative position, single one, array of holes, staggered rows, etc), l is the characteristic length (l = d for round circular jet and l = b for slot jet), α is the angle between jet row and an horizontal plane; β is the angle between two successive jet rows, γ is the jet impingement angle, e is the piccolo tube eccentricity, P_{jet} is the jet pressure, P_{atm} is the atmospheric pressure, $Ec = \frac{V^2}{c_p \Delta T}$ is the Eckert number and bc is the boundary condition on impingement wall.

The main dimensionless parameters that often appear in the Nusselt number correlations are: Mach number, Reynolds number, Prandtl number, impinging surface distance-to-jet diameter ratio and jet spacing-to-diameter ratio. The correlation proposed by Zaparoli et al. (2006) does not take account the effects of independent variations of Reynolds number. Therefore, the main objective at the present work is to evaluate the effect of the Reynolds number in the heat transfer process on the anti-icing protection system in the aircraft design.

To accomplish with this objective, the numerical simulations were performed using different jet hole diameters. This is due to the fact that a change in the fluid velocity will also affect the Mach number and that a change in the fluid properties (fluid density or fluid dynamic viscosity) will not be representative (the only fluid used on the anti-icing protection system is air). Therefore, just a variation on the hole diameter can take account the effect of independent Reynolds number variation.

The following jet hole diameters were studied: 1.50 mm, 3.00 mm, 4.50 mm, 5.25 mm and 6.00 mm. This range was selected to accomplish with the size of real hole diameters used in typical aircraft anti-icing protection system and the diameter used for the validation case (6.35 mm).

As the validation case the numerical simulation was performed using a Mach number equal to 0.4 and a jet inlet static temperature T_{in} = 300 K, which correspond to a total temperature T_T = 309.6 K a total relative pressure of P_{TR} = 11,809.6 Pa at the inlet. The impinging surface was maintained with a constant temperature T_w = 280 K. The distance between nozzle exit and the impingement plate was $z_n/d = 6$ and the spanwise distance between two holes was $c_n/d = 4$. The parameter c_n/d is different from the validation case $\left(c_n/d = 16\right)$ to be compatible with the values used in real anti-icing protection systems.

Each case is solved using three meshes as presented in Tab. 4. The simulations were carried on a common PC, which has a single Intel Pentium processor, 1G memory and 80G hard disk. The computation takes approximately 4 hours for the coarse meshes and 48 hours for the refined meshes.

Table 4 – Number of cells of the geometries studied

d (mm)	Number of cells		
	Coarse	Intermediate	Refined
1.50	119,460	261,251	445,506
3.00	100,011	222,136	403,034
4.50	108,468	242,785	447,612
5.25	235,257	440,482	703,823
6.00	119,460	261,251	478,107

Maximum and average Nusselt numbers are presented for Reynolds number range of 1.3x104 to 5.3x104 in Tab. 5. The maximum Nusselt numbers illustrate the non-uniformity of the heat transfer characteristic and provide support to understanding the average Nusselt number variations. The average Nusselt number data is more desirable than the local Nusselt number because the average number is less sensitive to experimental and numerical errors and thus more reliable for engineering design. Regarding numerical errors, they can be attributed to different factors: mesh quality, near wall treatment, discretization schemes, turbulence model employed, convergence criteria, etc.

Table 5 – Local maximum and average Nusselt number results

			Mesh		
d (mm)	Re	Nu	Coarse	Intermediate	Refined
1.50	1.33×10^4	Average Nusselt Number	8.80	8.62	8.66
		Difference	1.64%	-0.47%	0
		Maximum Nusselt Number	87.31	99.65	98.22
		Difference	-11.10%	1.46%	0
3.00	2.65×10^4	Average Nusselt Number	19.25	18.59	18.43
		Difference	4.42%	0.82%	0
		Maximum Nusselt Number	151.59	160.96	172.14
		Difference	-11.94%	-6.49%	0
4.50	3.98×10^4	Average Nusselt Number	25.70	26.60	26.09
		Difference	-1.49%	1.97%	0
		Maximum Nusselt Number	240.16	204.46	224.84
		Difference	6.81%	-9.06%	0
5.25	4.64×10^4	Average Nusselt Number	28.87	29.10	30.15
		Difference	-4.25%	-3.49%	0
		Maximum Nusselt Number	213.44	226.17	238.67
		Difference	-10.57%	-5.24%	0
6.00	5.30×10^4	Average Nusselt Number	33.67	32.58	32.59
		Difference	3.30%	-0.05%	0
		Maximum Nusselt Number	317.11	306.32	306.64
		Difference	3.41%	-0.10%	0

It is observed that average Nu is weakly dependent from mesh refinement while the maximum Nu values are more sensible to mesh refinement near the impinging surface wall or to y^+ variation.

Figure 5 shows the average Nusselt number results versus the Reynolds number for the refined mesh presented in Tab. 5.

The average Nusselt number related to the Reynolds number presents a correlation factor $R^2 = 0.9949$. Using a curve fitting minimizing the sum of squares of deviations, the correlation obtained was:

$$\overline{Nu} = 2.1154\, Re^{0.4825} \tag{16}$$

It is important to notice that this equation is valid for Ma = 0.4.

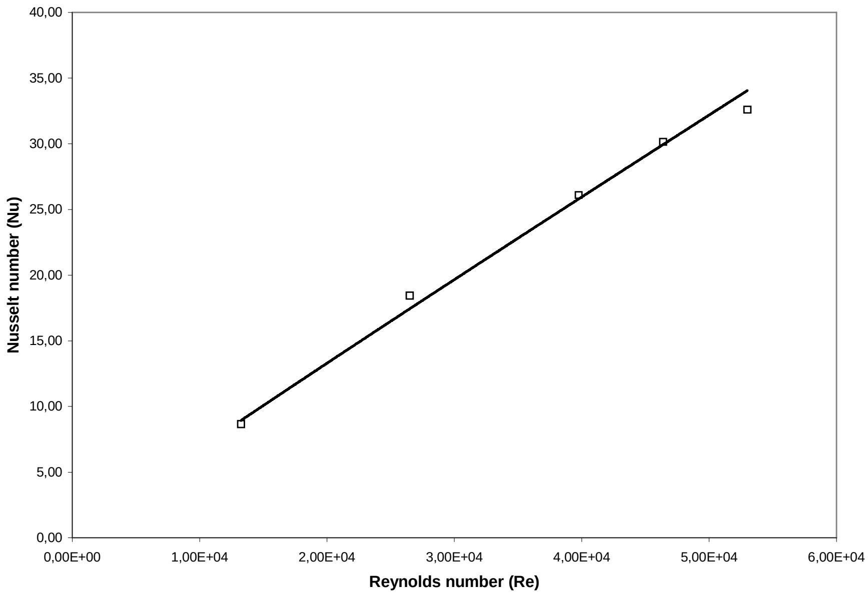

Figure 5 – Average Nusselt number results

4. FINAL COMMENTS

An aircraft wing thermal anti-icing protection system has been represented with a three-dimensional CFD simulation. The solutions were obtained for a simplified configuration: a single array of round jet impinging on a concave surface. A validation case shows good agreement with a numerical study realized by Zaparoli et al. (2006) and a correlation for the average Nusselt number considering the effect of the Reynolds number have been established.

5. ACKNOWLEDGEMENTS

The authors are grateful to FINEP (Financiadora de Estudos e Projetos (grant #01-04-0663-00) by the financial support to develop this work.

6. REFERENCES

CAA- Civil Aviation Authority, 2000. “Aircraft Icing Handbook”.

Ekkad, S., Huang, Y., Han, J.C, 2000. “Technical Notes: Impingement Heat Transfer Measuremen under an Array of Inclined Jets”. Journal of Thermophysics and Heat Transfer, Vol. 14.

Fregeau, M., Saeed, F., Paraschivoiu, I, 2005. “Numerical Heat Transfer Correlation for Array of Hot-Air Jets Impinging on 3-Dimensional Concave Surface”. Journal of Aircraft, Vol. 42, pp. 665-670.

Gau, C., Chung, C. M, 1991. “Surface Curvature Effect on Slot-Air-Jet Impingement Cooling Flow and Heat Transfer Process”. Transactions of the ASME, Vol. 113, pp. 858-864.

Goldstein, R. J., Timmers, J. F, 1982. “Visualization of Heat Transfer from Arrays of Impinging Jets”. International Journal of Heat and Mass Transfer. Vol. 25, pp. 1857-1868.

Huber, A. M., Viskanta, R, 1994. “Effect of Jet-Jet Spacing on Convective Heat Transfer to Confined, Impinging Arrays of Axisymmetric Air Jets”. International Journal of Heat and Mass Transfer. Vol. 37, pp. 2859-2869.

Lee, J., Lee S. J., 1999. “Stagnation Region Heat Transfer of a Turbulent Axisymmetric Jet Impingement”. Experimental Heat Transfer, Vol. 12, pp. 137-156.

San, J. Y., Lai, M. D, 2001. “Optimum Jet-to-Jet Spacing of Heat Transfer for Staggered Arrays of Impinging Air Jets”. International Journal of Heat and Mass Transfer, Vol. 44, pp. 3997-4007.

Shih, T., Liou, W. W., Shabbir, A., Yang, Z., Zhu, J, 1995. “A New Eddy Viscosity Model for High Reynolds Number Turbulent Flows”. Computers Fluids, Vol. 24, pp. 227-238.

Tawfek, A. A, 2002. “Heat Transfer Studies of the Oblique Impingement of Round Jets upon a Curved Surface”. Heat and Mass Transfer, Vol. 38, pp. 467-475.

Zaparoli, E. L., Andrade, C. R., Kurokawa, F. Y., Lima, R. C., Neves Jr., J. B. P, 2006. “Final Report – A8 Jet Flow”.

7. RESPONSIBILITY NOTICE